MODULATING PERFLUORINATED IONOMER FUNCTIONALITY VIA SIDECHAIN CHEMISTRY

Ashley Bird, [1,2] Matt Lindell, [3] Douglas I. Kushner, [1] Andrew Haug,[3] Mike Yandrasits,[3] A. Kusoglu[1,*]

[1] Energy Conversion Group, Lawrence Berkeley National Laboratory (LBNL), Berkeley, CA, 94720 USA

[2] Department of Chemical and Biomolecular Engineering, University of California, Berkeley, CA 94720 USA

[3] 3M Company, 3M Center, St. Paul, MN 55144, USA

*E-mail: akusoglu@lbl.gov

Abstract

Ionomers are important to electrode function in energy conversion devices, such as fuel cells and electrolyzers, as the catalyst-binding nanometer-thick films under confinement, which compromises mass transport of species. Mitigating confinement effects is necessary for improved performance of polymer electrolyte fuel cells. Studies on perfluorosulfonic acid (PFSA) ionomers provided insights into origins of transport resistances, but limited improvements by current strategies necessitates a need for alternative chemistries to enhance film function. This work investigates new ionomers based on sidechain modifications of PFSA to tune local acidity and structure. We systematically characterize their application-relevant properties (hydration, thermal-transition) and nanomorphology using environmental ellipsometry and grazing-incidence x-ray scattering, respectively, to develop chemistry-structure-property relationships in thin-film motif (≤100 nm). Introducing acid sites to sidechains improve hydration and nano-phase-separation but reduce chain mobility. Replacing the hydrophilic end-groups with hydrophobic perfluoro-groups enhances mobility but disrupts phase-separation. Although modifying sidechain functional groups alters ionomer-substrate interactions (Pt/C), chemistry has greater influence on structure-properties. Proton conductivity correlates with hydration, regardless of chemistry. This work improves the fundamental understanding of chemistry-function relationships of ionomers by providing a novel means to independently control their side-chain vs. end-group and observe resulting effects on interfacial properties to modulate electrode function in electrochemical technologies.

Keywords: Interfacial Interactions; Fuel Cells; Thin Films, GISAXS, Structure-Transport, Functional Coatings

TOC Graphic

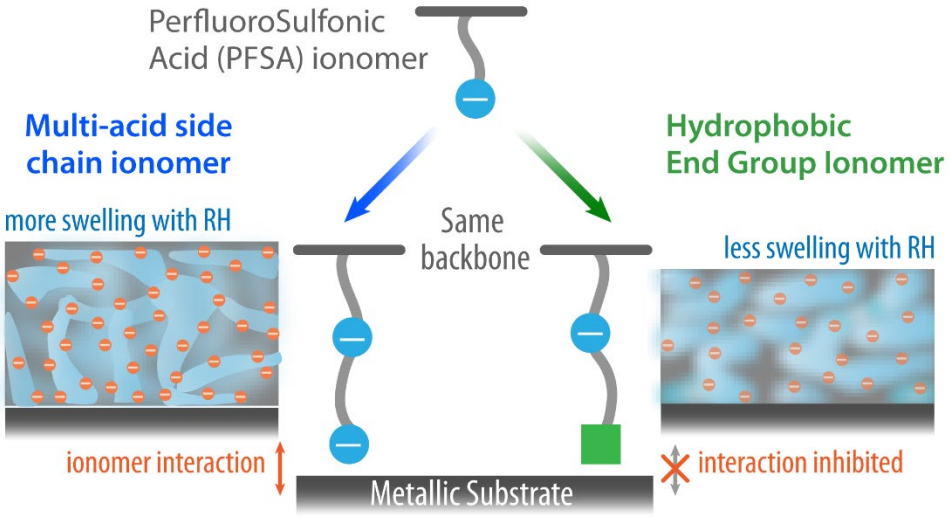

1. Introduction

Ion-conducting polymers (ionomers) have become an increasingly crucial class of materials due to their use in energy conversion devices, such as polymer electrolyte fuel cells (PEFCs), electrolyzers, and flow batteries.[1-3] Ionomers are used as separator membranes between electrodes as well as the catalyst-binding electrolyte in the electrodes of these devices. In the electrode, ionomers exist as nanometer-scale thin films enabling the transport of reactive species to and from catalyst sites (Figure 1). In the cathode catalyst-layer (CL) of fuel cells, for example, ionomer thin films play a key performance role by facilitating proton (ion) and oxygen (gas) transport for the oxygen reduction reaction (ORR).[1, 4] However, transport limitations through the ionomer thin film in cathode CLs limit PEFC performance (Figure 1).[5-11] The origins of these limitations are rooted in (i) confinement-driven changes in properties of ionomer thin film (compared to bulk membrane), and (ii) catalyst-ionomer interactions modulated by the ionomer's pendant chain and ionic groups. Thin film and CL studies show an ionomer under confinement exhibits densification, reduced water uptake, and increased mass transport resistance.[3, 10, 12-16] In the last decade, a great deal of effort has been expended to understand the underlying origins of transport resistances in perfluoro sulfonic acid (PFSA) ionomer thin films, which is key to improve efficiency and performance in fuel cells.[1] However, limiting focus to prototypical PFSAs (e.g., Nafion) narrows the fundamental understanding gained on the impact of ionic groups on mass transport. Furthermore, there is a lack of guidance for alternative chemistries that could offer materials solutions tailored to desired functionality for mitigating electrode resistances.

Perfluoro sulfonic acid (PFSA), the most widely studied ionomer chemistry, has a polytetrafluoroethylene (PTFE) backbone and sidechains terminating sulfonic acid groups. Due to the dissimilarity between the backbone and sidechains, hydration drives nano-phase separation into semi-crystalline hydrophobic domains and hydrophilic domains.[3] The hydrophobic PTFE backbone lends mechanical and chemical integrity, while the hydrated ionic network facilitates proton transport. One approach to improving functionality is to design ionomers based on PFSA by altering the backbone chemistry[17] or by increasing the ion exchange capacity (IEC),[18-20] which is inversely related to equivalent weight (EW). Previous work on PFSA has explored the effect of side chain length and number of polytetrafluoroethylene (PTFE) repeat units (m_{TFE}) between sidechains to modulate IEC (Figure 1).[2-3, 21] The greater concentration of ionic sites in high-IEC (low-EW) ionomers enables increased water

uptake and conductivity (Figure 1). However, reducing m_{TFE} to below 3-4 disrupts crystallinity, risks ionomer dissolution and washout in the CL and pore flooding.[3, 22] Additionally, increasing IEC in CL ionomers negatively impacts cell performance by increasing sulfonate adsorption to Pt catalysts sites, inhibiting reactive sites (referred to as "ionomer poisoning").[11, 23-24] Thus, improvements to PFSA ionomer functionality are constrained by IEC alone (Figure 1).

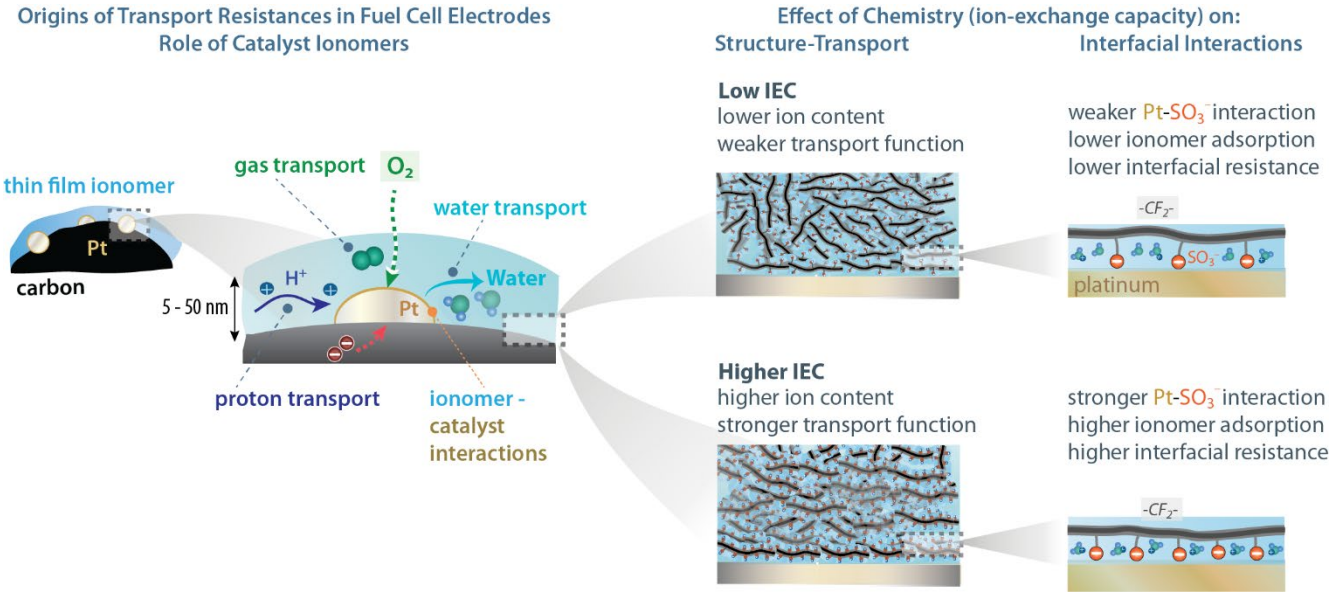

Figure 1. Effect of chemistry on catalyst ionomer function with the competing effect of ion-exchange capacity (IEC) on increasing ion content and transport function while also promoting the absorption of ionic groups onto Pt (catalyst) surfaces.

One way to overcome this limitation is the insertion of acid groups in sidechains, which increases the acid group concentration without compromising the level of sulfonate adsorption from pre-existing sulfonic acid groups to Pt (Figure 2). Additionally, acids in less accessible regions of the polymer may mitigate adsorption to Pt.[24] This strategy has been shown to result in increased water uptake and proton dissociation in membranes, especially at lower humidities, and achieve higher ionic network strength.[21-22, 25-26] However, such a class of multi-acid ionomers have not been examined fully in thin film form relevant to CLs. Moreover, these ionomers could be bound by the same trade-off between performance and poisoning related to IEC (Figure 1). Effectively improving ionomer thin film function without

destabilizing the material or compromising catalyst sites is presently difficult due to a lack of a fundamental understanding of the relationship between ionomer chemistry, structure, and properties. This work aims to evaluate new ionomer chemistries with independently-controlled sidechain functional and end groups to enable a better fundamental understanding of how the chemistry impacts ionomer properties, as well as how these properties change under confinement, and ultimately lead to a more tailored design of improved ionomers and interfaces.

This study systematically explores emerging and novel chemistries for catalyst ionomers designed following two potential strategies to improve thin film function: (1) increasing IEC by adding multiple acids per sidechain and (2) increasing the hydrophobicity of the sidechain terminus. The ionomers in this study have different EWs to maintain constant m_{TFE} across chemistries, using 3M PFSA (825 EW) as the reference material (Figure 2). The first series of *multi-acid sidechain (MASC)* ionomers include perfluoro ionene chain extended (PFICE) ionomers: PFICE-2 (aka PFIA, 620 EW) and PFICE-3 (aka PFICE, 540 EW) where the numerical suffix refers to the total number of acids (sulfonic or sulfonimide) per sidechain. The material strategy for the MASC series relies on increasing the number of acids per sidechain, and therefore the number of solvation sites, without sacrificing the backbone stability (m_{TFE}) and crystallinity. Thus, these ionomers are expected to have increased water uptake and conductivity in thin films while mitigating dissolution. While previously studied as membranes,[21-22, 25-26] it is necessary to probe thin film behavior of these multi-acid chain chemistries to understand the CL ionomer properties. The second series studied are *hydrophobic end group (HPEG)* ionomers, which include two novel chemistries: perfluoro-methyl imide (PFMI) ionomer (1050 EW) and perfluoro-butyl imide (PFBI) ionomer (1253 EW). Increasing the hydrophobicity of the sidechain terminal group reduces the interaction between acid groups and Pt and eliminate sulfonate adsorption. The final novel ionomer of this study is perfluoro-butyl-ionene chain extended (PFBICE-2) ionomer (697 EW), which has both ionene side-group and a hydrophobic end group to probe the relative influence of the two modification strategies.

This paper accomplishes two key objectives: (1) developing structure-property relationships of these ionomers with side-chain and end-group variations provide new fundamental insights into the role of ionic groups on thin film function that were otherwise/previously not accessed in studies limited to

PFSAs, and (2) provide synthesis and design guidelines for chemical tuning of ionomer structures for catalyst functions in electrochemical applications.

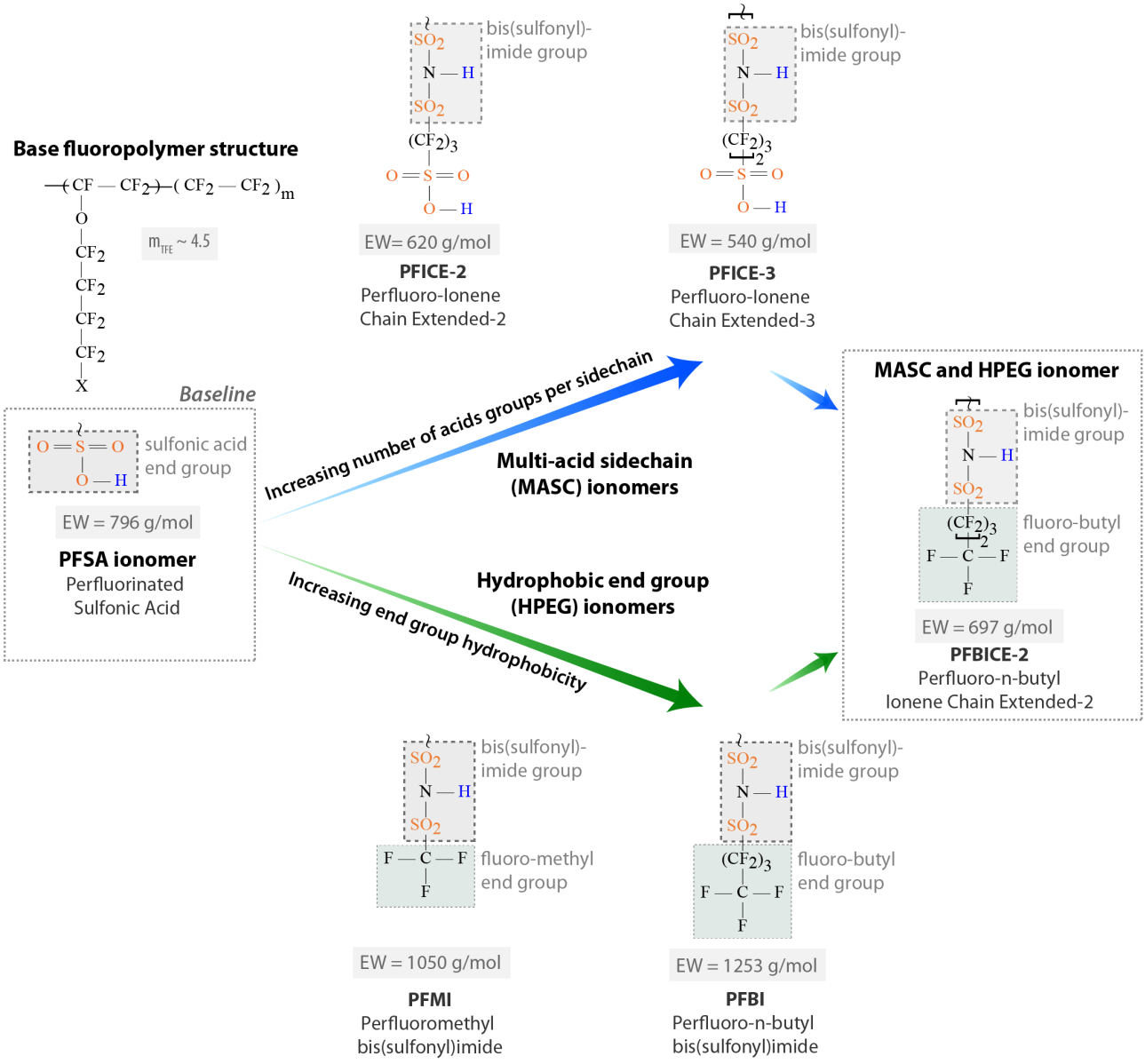

Figure 2. Ionomer chemical structures. 3M PFSA (796 EW) structure-property relationships are used as the baseline. MASC ionomers include PFICE-2 and PFICE-3 to investigate increasing the number of acid groups per side chain while maintaining the same SO_3 end group. HPEG ionomers include PFMI and PFBI to investigate increasing the end group hydrophobicity. PFBICE-2 is used to compare the relative impact of these modification strategies.

The paper is organized as follows: First, water uptake, which has implications for film conductivity, and thermal transition temperature, which is related to chain mobility, are presented. Nanomorphology is probed using grazing-incidence small- and wide-angle x-ray scattering (GISAXS/GIWAXS) and related to chemistry and property information. Then, the impact of side chain chemistry on the ionomer-catalyst interaction is investigated by characterizing thin films cast on metallic (Pt) and carbon substrates, which model the catalysts found in CLs. Finally, proton conductivity is measured and analyzed with hydration results to establish a structure-property map for ionomer functionality. The results are discussed to link the structure and functionality tuned by chemistry to provide insight on the relationship between chemistry and ionomer functionality and enable a more informed approach to ionomer design.

2. Methods

2.1 Materials

3M PFSA was obtained from 3M as a 25 solids wt. % dispersion in 25:75 water:ethanol mixture. 3M ionomers containing one or more bis(perfluoroalkylsulfonyl)imide groups per sidechain were synthesized by post-polymerization modification steps starting from the sulfonyl fluoride form precursor to 3M 825 PFSA in 3M Corporate Research Materials Laboratory (St. Paul, MN). Ionomers containing sidechains with a single bis(sulfonyl)imide were terminated with either perfluoromethyl (PFMI), perfluoro-n-butyl (PFBI), or sulfonic acid (PFICE) groups. Ionomers with multiple bis(sulfonyl)imides per sidechain, designated as ionene chain extended, were terminated with perfluoro-n-butyl (PFBICE-2) or sulfonic acid (PFICE-3). Detailed syntheses of PFICE ionomers can be found in the Supporting Information of Su *et al*. [21] Stock dispersion of PFICE-2 contained 21.5 solids wt. % in 20:80 water:ethanol, and stock dispersion of PFICE-3 contained 13.07 solids wt. % in 40:60 water:n-propanol. Details of the synthetic steps for perfluoromethyl bis(sulfonyl)imide ionomer (PFMI) and perfluoro-n-butyl bis(sulfonyl)imide ionomer (PFBI and PFBICE-2) dispersions are provided in the Supporting Information. Equivalent weights (EW) of ionomers were determined by titration of ionomer membranes, and detailed information can be found in the Supporting Information (SI).

2.2 Thin film preparation

Ionomer dispersions were prepared by diluting the stock dispersions in n-propanol (nPA) and deionized water and stirred overnight. The solvent composition of the diluted dispersion was 50:50 wt.%

nPA:water. Ionomer wt.% was adjusted to achieve desired film thickness. Silicon and platinum substrates were cleaned by rinsing with water and isopropanol (IPA), drying with N_2, and treating with UV-ozone for 20 minutes. The carbon substrates were rinsed with water and IPA and dried with N_2. Immediately after cleaning, the dispersion was spun-cast onto the substrate at 3000 rpm for 1 minute. Then, the film was annealed at 150 °C under vacuum for 1 hour and quenched in air.

2.3 Hydration

Thin film hydration was assessed via dimensional swelling measurements. A spectroscopic ellipsometer (J.A. Woollam alpha-SE) was used to determine transient film thickness as a function of relative humidity (RH). Initial film thickness was determined by collecting the spectra prior to film deposition and after film deposition. The wave amplitude (Ψ) and phase shift (Δ) over the spectral range 380-900 nm was fit to a 2- or 3-layer model (Cauchy layer/SiO_2/Si, Cauchy layer/Pt, or Cauchy layer/C). Films were pre-conditioned by cycling relative humidity (RH) from 0-100-0% RH generated by mixing a dry N_2 gas stream with humid N_2 at the dew point in various ratios to target specific humidity values. Measurements were taken using a custom environmental chamber with fused silica windows positioned normal to the beam path. Transient thickness was measured as RH was ramped up from 0% to 100% and back down to 0% in 10% steps, holding for 30 minutes at each step. The thickness, L, was averaged over the last 10 minutes of each RH step during the hydration and dehydration cycles. The change in thickness ($\Delta \mathrm{L} = \mathrm{L} - L_0$) was normalized by the initial thickness at 0% RH, L, to generate swelling profiles. Water content was estimated assuming one-dimensional swelling and additive pure molar volumes, as previously described:[12-13, 27]

$$\lambda = \frac{\mathrm{mol\ H_2O}}{\mathrm{mol\ SO_3^-}} = \frac{\Delta \mathrm{L}}{\mathrm{L_0}} \frac{\rho_{\mathrm{H_2O}}/\mathrm{MW_{H_2O}}}{\rho_{\mathrm{ionomer}}/\mathrm{EW_{ionomer}}} \quad (1)$$

where ρ is density and MW is molecular weight. A dry density of 2.1 g/cm^3 was assumed for all ionomers.[27-28] Water volume fraction (ϕ_{H_2O}) in the film is also calculated:

$$\phi_{H_2O} = \frac{\Delta \mathrm{L}}{\Delta \mathrm{L} + L_0} \quad (2)$$

2.4 Thermal transition

The thermal transition temperature corresponding to the relaxation of ionic clusters (T_α) was calculated by measuring the transient film thickness during heating and cooling in a dry nitrogen

environment.[3, 15, 29] Film thickness was determined using spectroscopic ellipsometry as described above. Thin films (100 nm) were cycled twice from 30 °C to 200 °C and down to 30 °C at 1 °C/min. The first heating step is excluded from the T_α calculations due to water evolution.[15] T_α was calculated from the change in the thermal expansion rate. The thickness vs temperature profile at low temperature (30 °C-50 °C) and high temperature (175-200 °C) were fit to linear functions, where the slopes are the thermal expansion rates. T_α was determined by calculating the temperature at the intersection of the two linear functions (*i.e.*, the temperature where the thermal expansion rates change).

2.5 Grazing-Incidence X-ray Scattering (GIXS)

Nanomorphology was investigated using GISAXS/GIWAXS performed at beamline 7.3.3. at the Advanced Light Source (ALS) at Lawrence Berkeley National Lab (LBNL). The x-ray energy was 10 keV with a monochromator energy resolution of *E/dE* of 100, and the sample-to-detector distance was 2 m and 0.3 m for GISAXS and GIWAXS, respectively. An incidence angle of 0.18, above the critical angle of the ionomer, was used. GISAXS measurements were collected under humidified (~95% RH) conditions using an in-house built environmental chamber to probe the nanophase separation. Linecuts of the 2D scattering images were corrected for background scattering, and the scattering (ionomer) peak was fit to a Gaussian function to extract domain spacing and full-width half-max (FWHM). Orientation of the ionic domains was assessed by calculating an orientation parameter (OP) using the method previously described.[11, 30] Briefly, the ionomer peak was azimuthally integrated to generate a pole figure. OP was calculated using the following equation[31]:

$$\mathrm{OP} = \frac{\int I(\chi)\sin(\chi)\,\cos^2(\chi)\mathrm{d}\chi}{\int I(\chi)\sin(\chi)\,\mathrm{d}\chi} \qquad (3)$$

where χ is the azimuthal angle. GIWAXS measurements were conducted under helium to probe the crystalline structure. Using horizontal linecuts, the crystalline peak and amorphous halo were fit using a double Gaussian function.

2.6 Inter-digitated electrode fabrication

Planar inter-digitated electrodes (IDEs) were fabricated to measure thin film conductivity. IDEs are defined by the number of teeth (N = 75), teeth width (4 μm), electrode spacing (d = 4 μm), and overlapping distance of the electrode teeth (t = 894 μm) (Figure S1). To fabricate IDEs, 400 nm thermal oxide layers were grown on Si wafers. MiR701 i-line photoresist was spin coated onto the wafer, and

the IDE pattern was written. Patterned areas of photoresist were removed using a MF-26A developer. Using a plasma etcher, 120 nm of the SiO_2 layer was etched. The etched volume was backfilled first with a 5 nm Ti adhesion layer, and the remaining volume was filled with Pt by electron-beam evaporation. NMP (n-methyl-2-pyrrolidone) was used to remove excess metal and photoresist. The wafer was then diced and rinsed with acetone, followed by the above cleaning and thin film fabrication procedure.

2.7 Electrochemical properties

Potentiostatic electrochemical impedance spectroscopy (PEIS) using a potentiostat (Bio-Logic VSP-300) to determine thin film conductivity. Dispersions were prepared as described above with a final solvent composition of 10:90 wt.% water:nPA to have a controlled composition that is comparable to previous thin film conductivity studies.[32-34] 50 nm thin films were prepared as above and cast onto fabricated IDEs (Figure S1). To measure the film resistance as a function of humidity, the film was first pre-conditioned by cycling the RH from 0% to 100% to 0% RH. The humidity was then increased from 0% RH to 100% RH in intervals of 10% RH, allowing the film to equilibrate at each step for 30 minutes (with the exception of 100% RH which equilibrated for 45 minutes) before data collection. The potential oscillation frequency ranged from 1 MHz to 0.1 Hz with an amplitude of 10 mV. Three measurements were collected at each RH, resting 5 minutes between measurements. The spectra were fit to the following equivalent circuit model to extract film resistance (R)[33, 35] with the model fit overlaid on the measured impedance of the samples, as shown in Figure S2.

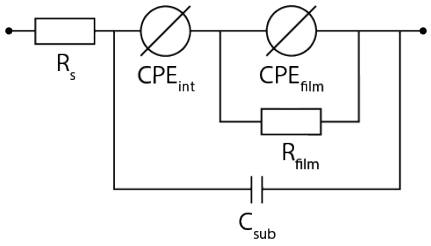

Figure 3. Equivalent circuit model used to extract thin film resistance. R_{film} represents the film resistance, R_s represents the intrinsic experimental set up resistance, and C_{sub} represents the capacitance of the silicon oxide substrate. CPE_{int} and CPE_{film} are constant phase elements that describe the film-substrate interface and film, respectively.

The following equation developed for thin films was used to calculate proton conductivity (κ):[33, 35]

$$\kappa = \frac{1}{R}\frac{d}{t(N-1)L} \quad (4)$$

The film thickness (L) was measured at each humidity using SE. Note that at sufficiently low RH, the film resistance was not resolvable using the equivalent circuit model, and the humidity cutoff for resolving resistance varied by chemistry. Using the extracted conductivity and dimensional swelling, proton concentration (c_{H^+}) and mobility (μ'_{H^+}) were calculated using the following equations[36]:

$$c_{H^+} = \frac{n_{H^+}}{V} = \frac{\rho_{ionomer}}{EW_{ionomer}} \cdot \frac{1}{1+\frac{\Delta L}{L_0}} \quad (5)$$

$$\mu'_{H^+} = \frac{\kappa}{F \cdot c_{H^+}} \quad (6)$$

where $\boldsymbol{n_{H^+}}$ is the moles of protons, $\boldsymbol{V}$ is the total hydrated film volume, and $\boldsymbol{F}$ is Faraday's constant.

3. Results and Discussion

3.1 Hydration

Improving film function at low humidities is important for expanding the humidity range for efficient operation of fuel cell electrodes, especially at elevated temperatures. Ionomer hydration (water uptake) impacts reactive species transport for HOR (hydrogen oxidation reaction) and ORR in fuel cells.[11, 18, 37-40] Hydration is driven by the absorption of the water molecules by the ionomer's ionic sites where initial water molecules solvate the ionic sites at low humidities. As humidity increases, subsequent water molecules form a secondary hydration shell around the ionic site. More water molecules lead to coalescence of ionic clusters, forming the hydrophilic (or ionic) network, which facilitates water and proton transport through the ionomer.[3] Additionally, oxygen transport is also reduced at low humidities.[41-42] Thus, improving water uptake of ionomers is a method to improve domain connectivity and mass (H^+, O_2) transport at lower humidities. In thin films, volumetric swelling due to water sorption is characterized by measuring film thickness over a humidity range using *in situ* spectroscopic ellipsometry (SE) to determine dimensional swelling.[43-45]

Figure 4a shows the swelling profiles of 100 nm films cast on Si. In the MASC series, dimensional swelling increases across the RH range with an increasing number of acids per side chain. PFICE-2 and PFICE-3 swell more than PFSA, suggesting that these films absorb more water due to the greater concentration of solvation sites. To account for the differences in IEC, Equation 1 is used to calculate water content (λ), a measure of local hydration in terms of the number of water molecules per acid site.[3] Swelling trends are also observed in λ, albeit with weaker difference among the ionomers (Figure 4b),

suggesting the hydration mechanism or domain formation are different in these new chemistries. Density functional theory (DFT) simulations by Su et al. indicated water molecules are shared between solvation sites on the sidechains in PFICE ionomers, which may contribute to the higher λ.[21] Interestingly, PFICE-2 and PFICE-3 have comparable swelling despite PFICE-3 having a higher IEC. While comparable water uptake for PFICE ionomers was previously observed for membranes,[21] these results demonstrate the trend is maintained for thin films under confinement. Additional solvation sites in MASC ionomers enable greater water uptake in thin film form than PFSA. However, the comparable swelling of PFICE ionomers suggests other phenomena impact swelling since PFICE-3 has a higher IEC than PFICE-2. So, higher IEC in MASC does not always translate into higher swelling. One possibility is the accessibility of the solvation sites; the imide group nearest the backbone may be less accessible to water molecules. Alternatively, stronger chain-chain interactions or film crystallinity may inhibit deformation and chain mobility, thereby reducing the hydration gain expected from the presence of the additional solvation site.[15] Previous work has shown increasing crystallinity through thermal annealing or morphological changes could reduce water uptake.[45-48]

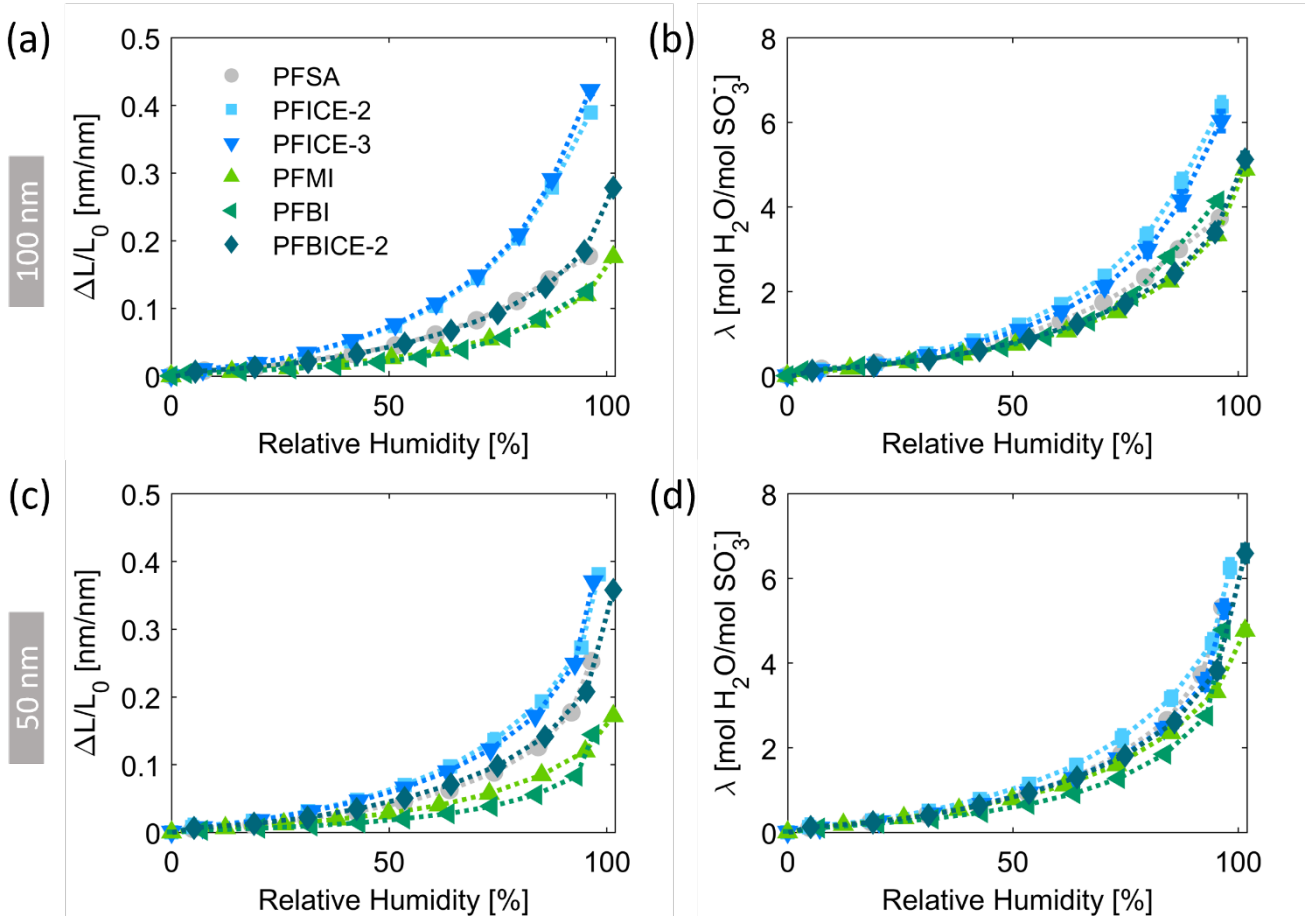

Figure 4. Water uptake of ionomer thin film cast on Si at room temperature. (a) dimensional swelling and (b) water content, λ profiles of 100 nm films and (c) dimensional swelling and (d) λ profiles of 50 nm films of MASC and HPEG chemistries compared to 3M PFSA ionomer. Increasing the number of acids per side chain increases the water uptake, while increasing the length hydrophobic end group reduces water uptake.

In the HPEG series, swelling decreases as the end-group hydrophobicity increases (Figure 4). The hydrophobic end groups may reduce accessibility of the acid group or disrupt the hydrophilic domain formation and/or connectivity. PFBICE-2, which has two acids per side chain and a bulky end group, has comparable swelling to PFSA, suggesting that multi-acid sidechains and hydrophobic end group influences the water uptake similarly but with opposite effect (increasing and decreasing, respectively).

Swelling and water content (λ) profiles of thinner films (50 nm) were also measured to understand the interplay between chemistry and confinement (Figure 4c-d). Swelling of 50 nm films showed the same trends with chemistry as with 100 nm films, indicating that sidechain chemistry is a more dominant factor on water uptake across the range film thicknesses examined here (Figure 4c). However, the λ profiles appear to collapse into a single profile for 50 nm films, differing from thicker 100 nm films (Figure 4d). The stronger confinement may hinder different hydration mechanisms and domain formation in the MASC and HPEG ionomer such that IEC becomes the main driving force for hydration. Alternatively, the density is assumed to be uniform and constant at 2.1 g/cm^3, which is commonly used for PFSAs,[27-28] but this assumption may not hold under varying degrees of confinement and for the varying sidechain chemistries. Additionally, molecular dynamics simulations suggest densification near the ionomer-substrate interface.[10, 16] Quantification of thin film density and density profiles are challenging and may be determined from simultaneous quartz-crystal microbalance (QCM) and SE measurements and X-ray or neutron reflectometry, respectively.[17, 49-51] To test the effect of ionomer density on these results, we estimate 10% uncertainty for the ionomer density and recalculated the error bars for the water uptake (SI Figure S3). The observed trends are maintained within at 10% uncertainty in density.

Comparing swelling of the two film thicknesses, all ionomers (except PFMI) showed reduced water uptake for thinner, 50 nm films due to greater confinement, as expected when ionomer film thickness is reduced.[12, 52] The hydrophobic end-group in PFMI likely reduce the ionomer-substrate interaction at the interface, mitigating nearby confinement effects (Figure S4). Reversing the confinement-driven reduction in swelling with end-group modification reveals a chemical strategy to tune hydration-driven function. However, this mitigation is not observed in PFBI or PFBICE-2, which may be attributed to their longer, more flexible sidechains. Techniques such as molecular dynamics (MD) simulations[10, 53-55], QCM[56-57], and electrochemical methods for MEAs[58-60] could provide insights into this interaction. Different material supports have also been used to understand the impact on thin film behavior.[13, 46, 61-63] The impact of the ionomer-substrate interaction and the role of the end group on thin film behavior are discussed next.

3.2 Thermal Transition Temperature

Chain mobility and free volume have implications for gaseous transport through the ionomer thin film.[17, 40, 64] Thus, thermal transition temperatures provide insight into these transport properties.[3, 15, 43] Ionomers have multiple thermal transitions associated with carbon-carbon bonds, backbone, and ionic moieties. The α-transition temperature (T_α, usually 80°C-150°C) is associated with the relaxation of the ionic clusters.[15, 25, 29, 48] A higher T_α indicates a stronger ionic network and reduced chain mobility because more energy is needed to overcome the intermolecular forces; conversely, a lower T_α indicates greater chain mobility. T_α of the MASC and HPEG ionomers was measured to understand the impact of chemistry on the ionic network and chain-chain interactions (see SI Figure S5).

Figure 5a shows T_α increasing as a function of the IEC for each chemistry, indicating increasing the sidechain charge density improves thermal stability and strengthens the ionic network. Although most literature on PFSA membranes indicate a reduced T_α with IEC, those studies were based on IEC variation due to both sidechain and length of TFE units in the backbone (m_{TFE}).[3] This work highlights changes in T_α due solely to side-chain modification for a fixed backbone length. In fact, the results for MASC ionomer thin films are consistent with previous work on PFICE membranes.[25] The increasing network strength with the number of acid sites for the same m_{TFE} could hinder chain mobility and increase resistance to swelling, which could explain why water uptake does not increase much for the PFICE-3 as discussed above (Figure 4). Additionally, the trends in T_α with IEC are consistent with trends in water uptake (Figure 5b), demonstrating the dependence of multiple ionomer properties on the chemical structure (i.e., IEC).

Interestingly, the relationship between T_α and IEC appears linear with different slopes depending on end group chemistry (sulfonic acid vs HPEG), suggesting these properties are coupled. Furthermore, the greater slope for chemistries with hydrophobic end groups suggests the end groups have a relatively greater impact on the nature of the ionic cluster interactions and ionic network, leading to greater sensitivity of T_α to IEC. To resolve the effect of chemistry on the ionic (hydrophilic) domains, thin film morphology is investigated next.

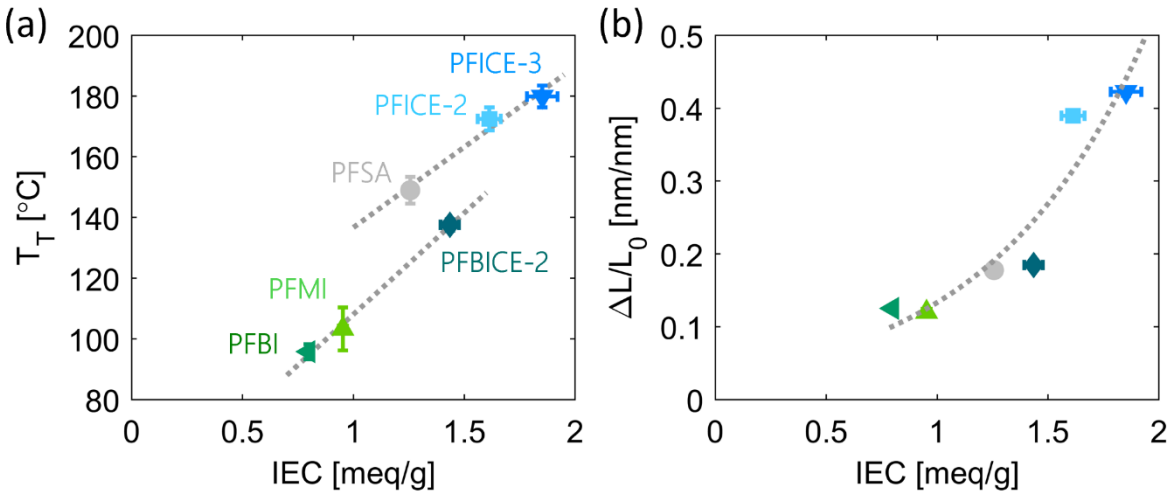

Figure 5. (a) Thermal Transition Temperature and (b) dimensional swelling at 95% RH (b) of various ionomer thin films plotted against their IEC. Dashed lines indicate trends to guide the eye. T_α and water uptake increase with IEC based on six chemistries investigated.

3.3 Nanomorphology

Nanomorphology is correlated with ionomer properties in thin film form, including water uptake and conductivity,[10, 12, 32, 43, 45, 60] and the sidechain chemistry impacts the nanomorphology.[3, 11, 21] For example, shorter side chains lead to lower crystallinity and greater nanophase separation.[11, 45] In perfluoroimide acid (PFIA) membranes, greater nanophase separation compared to PFSA has also been observed.[21, 48] To gain insight into the relationship between the MASC and HPEG ionomers and their exhibited film properties, nanomorphology is characterized via GIXS. GIWAXS captures the smaller, overlapping crystalline peak and amorphous halo at larger q (9-13 nm^{-1}), and GISAXS captures the larger hydrophilic domain spacings at smaller q (0.3-3 nm^{-1}). Horizontal linecuts of GIWAXS in helium shown in Figure 6 at larger q, and the peak fit results are tabulated in SI Table S1. The crystalline peak arises from the PTFE backbone (c. 12.7 nm^{-1}) and is impacted by m_{TFE}.[3] Due to the comparable spacing between sidechains, crystallinity is not strongly impacted MASC or HPEG modifications (See SI, Figure S6). As mentioned above, crystallinity affects film properties such as swelling.[45, 47] Crystallinity inhibits excessive deformation of the ionomer's mesoscale network, so the comparable semi-crystalline features may explain the comparable dimensional swelling profiles observed in the PFICE ionomers.

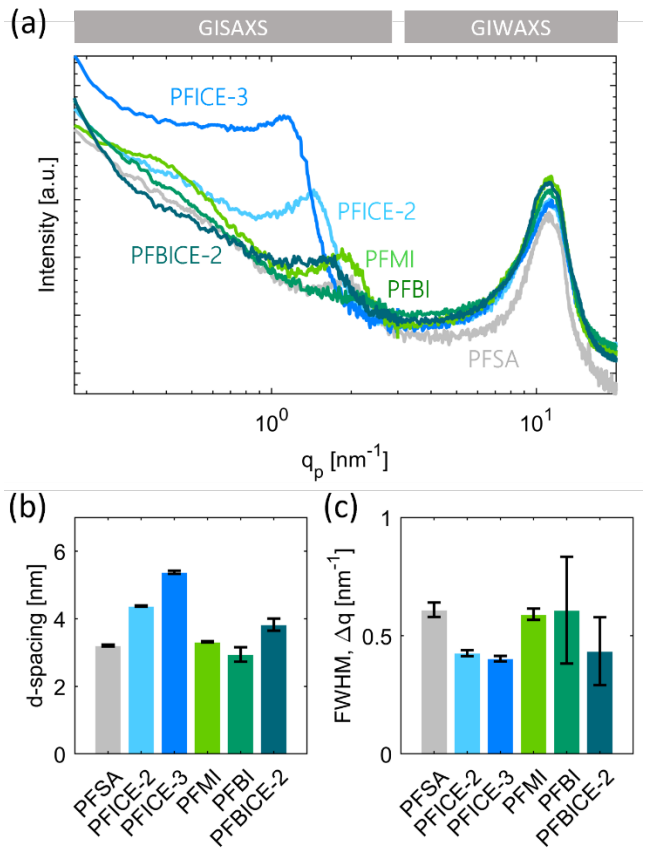

Figure 6. Morphology of 50 nm ionomer thin films as characterized by GIXS. (a) stitched horizontal linecuts of GISAXS in humidified nitrogen (95% RH) and GIWAXS in helium, (b) ionomer peak d-spacing, and (c) ionomer peak FWHM. D-spacing increases with sidechain length/acid location. Lower FWHM suggests a higher degree of phase-separation. Crystallinity does not change greatly as m_{TFE} is fixed between chemistries.

The hydrophilic nano-domains in phase-separated ionomer leads to a single scattering peak, termed the *ionomer peak*, observed via GISAXS at smaller q (0.7-2 nm^{-1}). The ionomer peak is analyzed to calculate the average hydrophilic domain spacing (d-spacing) and FWHM for all chemistries (Figure 6, also see SI Figures S7-S9). The FWHM describes the distribution of domain spacings and is dependent upon background scattering and the hydrophilic-hydrophobic domain interface (*i.e.*, nanophase separation). A narrower scattering peak, and thus a lower FWHM, suggests more uniform nanophase separation in the film. Comparing the MASC ionomers, d-spacing increases with increasing acid sites per sidechain. In conjunction with greater water uptake (Figure 4), these results suggest MASC ionomers

have larger, well-connected hydrophilic domains. However, PFICE-3 has a larger d-spacing compared to PFICE-2 but comparable water uptake, indicating that thin film d-spacing is driven more strongly by sidechain length and not solely hydration, in agreement with previous observations on membranes.[21] The reduced FWHM of MASC ionomers suggests that greater water uptake and/or MASCs leads to greater nanophase separation and/or local ordering within the film. It is noteworthy that adding more acid groups tend to increase domain spacing but with relatively minor impact on the degree of phase separation.

Film properties are impacted also by polymer-domain orientation.[46, 51, 65] For example, greater domain orientation improves proton conductivity in the direction parallel to the domains.[65] The orientation parameter (OP) of hydrophilic domains was quantified to better understand the influence of sidechain chemistry on orientation. Due to interference from the specular rod and the Yoneda peak, the OP was calculated over a truncated azimuthal range (χ), 4° to 70° from the vertical direction instead of 0° to 90°. For this range, the OP ranges from 0.117 to 0.995, and the isotropic case has an OP of 0.484. An OP approaching 1 arises from higher scattering intensity at lower χ, indicating domains are oriented parallel to the surface of the substrate ("through-plane alignment"). Similarly, an OP approaching 0 arises intensity at higher χ, indicating domains oriented perpendicular to the surface ("in-plane alignment"). Interestingly, the OP of all ionomers in thin film (except PFBICE-2) indicated isotropic domain orientation (SI Figure S10). The lack of orientation may be attributed to film processing. Because annealing the films allow chain rearrangement and may reduce observed anisotropy that may result from other processing steps (*e.g.,* spin coating).[13, 46, 66-67] As there were no differences in orientation between the ionomer chemistries, there may be important morphological features not captured by GISAXS, such as tortuosity, which may explain the relationship between water uptake and d-spacing. Direct imaging and MD simulations on PFSA provided insight into nanomorphology and may be helpful for understanding the nanomorphology of the MASC and HPEG ionomers.[10, 54-55, 68-69]

3.4 Ionomer-substrate interactions

In thin film research, Si is commonly used as the substrate as it is easy to obtain a clean, homogenous substrate to perform studies and compare to previous baseline. For example, Si contributes less to the scattering background compared to metals such as Pt. However, characterizing thin films on application-relevant substrates, such as Pt and C, would provide insight into the ionomer behavior in device

electrodes. For this reason, the impact of sidechain chemistry on the ionomer-catalyst interaction is probed by characterizing 50 nm thin films cast on Pt and C substrates.

Figure 7 shows dimensional swelling on Si, Pt, and C for selected chemistries. PFSA films swell differently depending on the substrate (interactions), with higher swelling on Pt and Si. Sulfonate preferentially interacts with Pt over the ionomer backbone, leading to a water layer at the interface and greater water uptake.[23-24, 55, 62-63, 68, 70] Compared to the hydrophilic moieties, the hydrophobic backbone preferentially interacts with C, leading to lower water uptake.[54, 63] Thus, the molecular constituents of an ionomer could modulate the changes in film properties due to substrate interactions which impact the swelling the most at high RH (>70%). PFICE-2 and PFBI films swell with much less dependence on substrate, demonstrating that these chemical modifications could lead to substrate-independent changes in certain properties (Figure 7). Similarly, increasing the density of acid groups also has greater influence over hydration than differences caused by the ionomer-substrate interactions.

HPEG may diminish the strength of the ionomer-substrate interaction since imide groups are less accessible at the interface. Notably, the chemistry trends observed on Si are present also on C and Pt (SI Figure 2). In other words, compared to PFSA, PFICE-2 swells more and PFBI swells less on all substrates, consistent with the hypothesis that sidechain chemistry has greater influence on dimensional swelling than ionomer-substrate interactions.

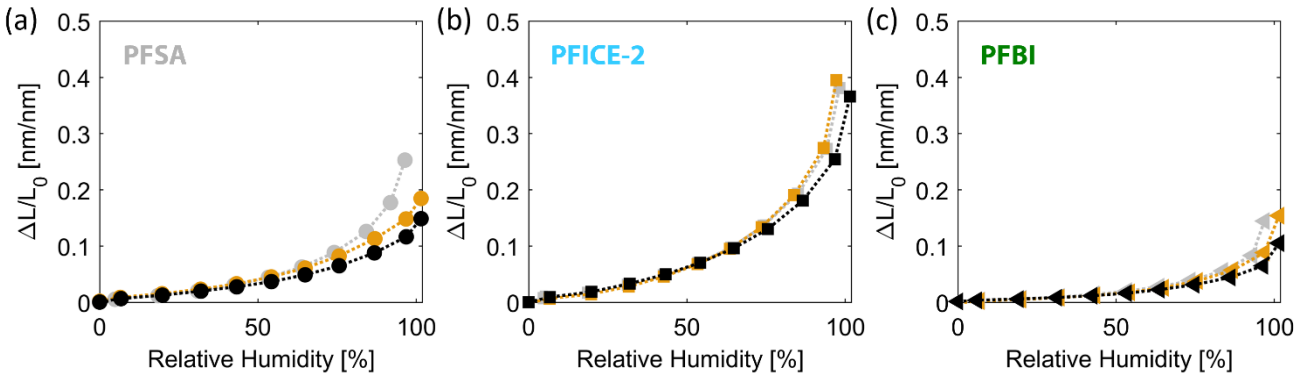

Figure 7. 50 nm films swelling profiles on Si, Pt, and C. Dimensional swelling on Si, Pt, or C substrates for (a) PFSA, (b) PFICE-2, and (c) PFBI. Swelling is more sensitive to chemistry than substrate.

Figure 8 shows the impact of ionomer-substrate interactions on morphological parameters characterized via GIXS. The d-spacings, FWHMs, and OPs calculated from the ionomer peak do not

change significantly with substrate, supporting the stronger influence of sidechain chemical modifications over ionomer-substrate interactions. Furthermore, increasing acids per sidechain to improve film function may not necessarily contribute to greater adsorption as one might expect in the presence of additional Pt-acid interaction sites because imide groups show weaker adsorption to Pt than sulfonate.[24] Previous work on PFSAs also suggests ionomer-substrate interactions and processing (*e.g.*, solvent, thermal treatment) influence adsorption and domain orientation.[11, 13, 46, 57, 66, 71-72]

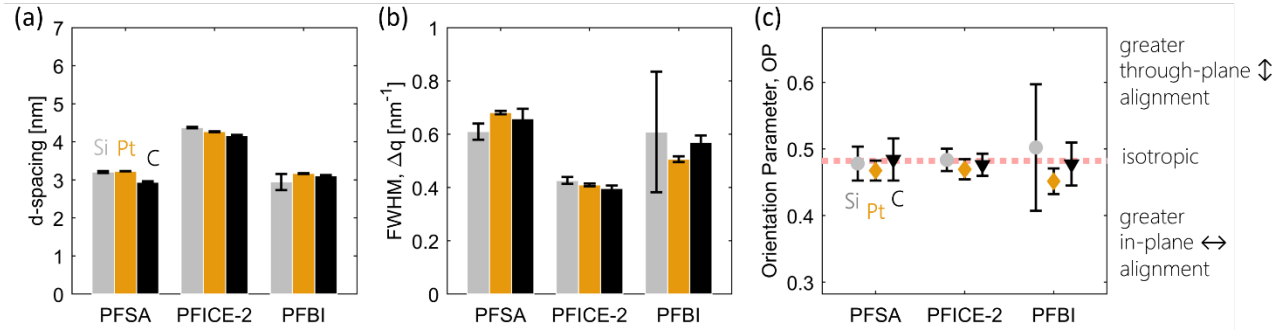

Figure 8. Morphological effects of ionomer-substrate interactions on select ionomer chemistries. Ionomer peak (a) d-spacing, (b) FWHM, and (c) orientation parameter (OP) of 50 nm films cast on Si, Pt, and C, and Ionomer sidechain chemistry has greater influence over film morphology than ionomer-substrate interactions. The OP demonstrates the hydrophilic domains are randomly oriented (isotropic).

3.5 Electrochemical properties and Conductivity

To assess the impact of sidechain chemistry on film function, proton conductivity (κ) profiles from 0% to 100% RH are determined via EIS of 50 nm thin films cast on IDEs. Inter-digitated electrodes (IDEs) greatly improve the sensitivity to thin film resistance by reducing the spacing—therefore the ohmic resistance—between electrodes. Figure 9a-b shows the thin film conductivity as a function of RH and water volume fraction (ϕ_{H_2O}) in the film. At low RH, films are not sufficiently conductive to resolve the film resistance from EIS. For most samples, film resistances were resolvable above 20% RH, but PFMI and PFBI were not resolvable until 30% and 65% RH, respectively. The low water uptake in these films at low humidity demonstrates the dependence of conductivity on hydration.

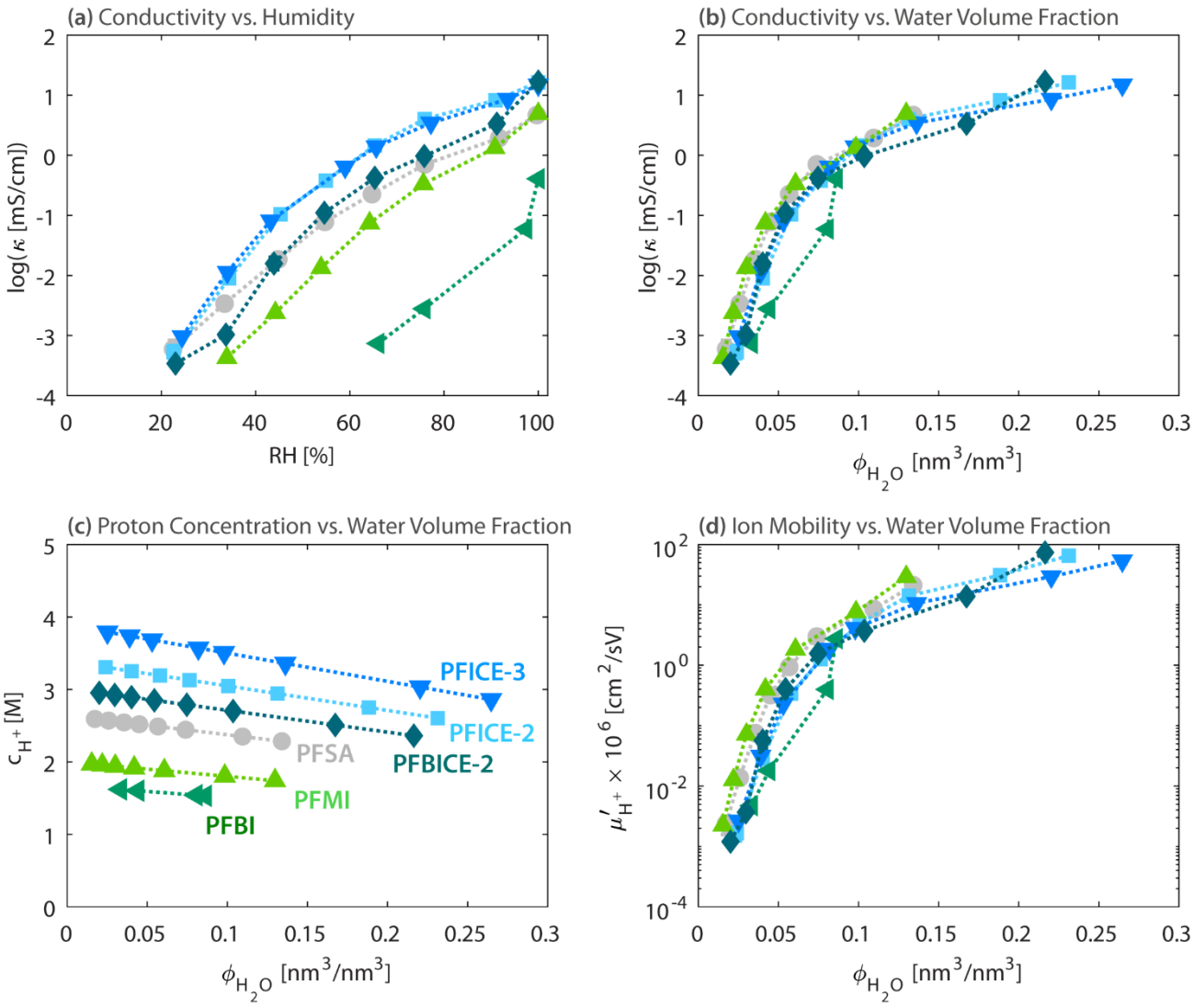

Figure 9. Film functionality. (a) Proton conductivity (κ) vs relative humidity (RH), (b) proton conductivity (κ) vs water volume fraction (ϕ_{H_2O}), (c) ion concentration (c_{H^+}), and (d) ion mobility (μ'_{H^+}). Symbols and colors are the same in all four plots, as labeled in (c)

Conductivity rapidly increases at high RH as water uptake increases, and similar trends in swelling are observed for both MASC series and HPEG series ionomers. Specifically, PFICE ionomers have comparable conductivity profiles and are more conductive than PFSA, whereas PFMI and PFBI have the lowest conductivities for a given humidity. Thus, for a perfluorinated ionomer with a given m_{TFE}, adding protogenic groups to sidechains enhances low-humidity conductivity (for MASC), while eliminating the end groups reduces it (for HPEG). This provides a chemical means to control humidity-

dependent conductivity of ionomers for CL because proton conduction is an important function of ionomer thin films for the HOR/ORR reactions occurring in CLs with varying degree of humidities.

Previous studies have attributed differences in water uptake and conductivity to the percolation and connectivity of hydrophilic domains.[3, 10, 73-76] As water absorbs into the film, the domains connect and form transport pathways to enable proton transport. The comparable conductivity and hydration for PFICE ionomers suggests the imide groups may not contribute significantly to concentration of dissociated protons. However, PFSA and PFMI have somewhat comparable conductivities at higher humidity (>70%) despite differences in dissociation between sulfonic acid and imide groups.[48] Dielectric spectroscopy studies of PFICE-2 (membranes) documented limited dissociation from the imide group, which interacts with the stronger sulfonate group via the intra- and inter-sidechain interactions to promote the proton delocalization and enhance mobility.[48] In PFICE-3, the second imide group nearest the backbone may be more inaccessible to water and hinder hydration and proton dissociation from this group instead. The poor conductivity of PFBI (Figure 10a) may be explained by their suppressed water uptake (Figure 4c) preventing proton dissociation below 60% RH as well as the bulky hydrophobic end groups disrupting formation/connectivity of the hydrophilic domain and/or increasing tortuosity. PFMI is less conductive than PFSA but 10-20x more conductive than PFBI, which has a bulkier HPEG and is therefore more disruptive to the hydrophilic network and the ion transport pathways (Figure 10a). While the hydrophobic end groups may reduce catalyst poisoning, their impact on film properties and structure could also compromise functionality.

4. Discussion

4.1 Establishing the Structure - Conductivity Relationship

To elucidate the underlying origins of conductivity changes with chemistry, the theoretical ion (proton) concentration (c_{H^+}) and mobility (μ_{H^+}) in the films are determined and correlated from conductivity and hydration results (Figure 9c-d). Ionomer films with higher IECs have greater ion concentrations. As ϕ_{H_2O} increases, the film swells, and ion concentration decreases. Ion mobility increases due to greater hydration enabling a shift from vehicular water transport to proton hopping, a much faster proton transport process.[3, 73-76] Interestingly, PFICE-3 has a greater ion concentration than PFICE-2 but does not have greater conductivity, leading to a lower calculated ion mobility, which supports the claims that the second imide group does not fully dissociate and contribute significantly to proton conductivity.[48] In fact, ion mobility even decreases with increasing IEC for these chemistries. At

ϕ_{H_2O} = 0.13 (c. 75-100% RH range), PFMI has the highest ion mobility at a given ϕ_{H_2O} while PFICE-3 has the lowest. *Therefore, increasing IEC alone does not necessarily improve proton mobility for a given hydration level, even though it does increase conductivity for a given humidity*. The latter effect, despite being a practical indicator for CL performance, does not fully capture fundamental transport mechanisms in ionomer thin films, the understanding of which has been thus far limited to PFSA ionomers that lack systematic chemical modifications.

Ionomer conductivity depends on water uptake because hydration promotes solvation of acid groups, proton dissociation, and enhances mobility of protons, while the hydrophilic network provides pathways for facile transport.[21-22, 48] At low humidity/λ values, the electron withdrawing nature of acid groups along with their separation distance (m_{TFE}) affects proton dissociation and the local acidity, which controls conductivity. For this reason, below λ = 6-7, proton transport in PFSA occurs mainly via surface mechanisms and vehicular transport of hydronium ions (H_3O^+).[3, 48, 74, 77] At higher humidity/λ values, with formation of water network, phase-separated morphology becomes more a dominant role in controlling conductivity by facilitating the proton-hopping.[3] Recent studies showed similar hydration-driven mechanisms also for PFICE membranes, but with the caveat that the additional imide group, despite its lower acidity than the end group, enhances conductivity at lower humidity by providing more protons.[21, 48] In addition, water molecules shared between solvation sites in MASC ionomers may impact the hydrophilic pathways.[21] In thin films, however, confinement reduces the λ to below 6 (see Figure 4), compromising the formation of a bulk-like water-network, which likely reduces contribution from hopping mechanism. In such a scenario for confined ionomers with low hydration, proton transport should be governed more by surface mechanism that is dependent on the (i) local acidity of sidechains, and (ii) sidechain separation distance (m_{TFE}), which is the same for all chemistries in this study. This could explain the relatively reduced spread in effective proton mobility across these chemistries (Figure 9d). At higher hydration, the nanomorphology and domain connectivity become a controlling factor in facilitating proton transport in the ionic water network.

In terms of morphology, the HPEG ionomers have comparable d-spacings to PFSA, despite its longer sidechain length. However, the solvation sites are in similar locations on the sidechain with respect to the backbone. These results indicate that d-spacing might be governed by the location of the most accessible acid on the sidechain with respect to the hydrophobic backbone. In other words, the hydrophilic domains are centered around the most accessible acid, where water molecules most readily

interact with ionic moieties. Importantly, d-spacing does not directly relate to observed property trends (*e.g.*, water uptake). When humidified, the HPEG ionomers absorb less water compared to PFSA, yet possess similar d-spacings and FWHM (degree of phase-separation). Water uptake depends more strongly on accessibility and the number of the solvation sites. Interestingly, PFBICE-2 has a hydrophobic end group but exhibits comparable FWHM to MASC ionomers, demonstrating the competing influence of the two modification strategies. The hydrophobic groups inhibit domain formation, but the addition of a second imide group increases interaction between hydrophilic groups and enables better domain formation/phase separation (i.e., lower FWHM for PFBICE-2 compared to PFMI/PFBI). These observations further indicate that it is possible to decouple the hydration-dependence of domain spacing and phase-separation to modify nanomorphology via sidechain chemistry.

Overall, hydration-dependencies of conductivities are consistent with previous thin film studies.[32-33] Our results with a wider range of chemistries suggest a strong universal relationship exists between proton conductivity and water uptake of ionomer films. When the conductivity is plotted as a function of ϕ_{H_2O}, all the curves collapse into a universal trend, indicating that the microscopic water fraction in the film is a strong indicator for proton conductivity.

4.2 The effect of side-chain vs. end-group modification

The MASC and HPEG ionomer films have different sidechain acidity (pKa values), and nano-morphology (Figure 6), which leads to different conductivity as a function of humidity, yet their effective conductivity exhibits a similar, almost universal dependence on water volume fraction. While this seems counterintuitive, a close examination of factors controlling conductivity could provide some insights:

- The overall proton activity is expected to decrease, MASC > PFSA > HPEG, due to the elimination of highly acidic SO_3^- groups in the latter. The water uptake at a given humidity also decreases in the same order, which can be interpreted as an increase in the amount of water molecules required to dissociate proteogenic groups: HPEG > PFSA > MASC. This explains the trends for humidity-dependent macroscopic conductivity, and why MASC PFICE could reach higher conductivity levels for a given RH (Figure 9a)
- Once an ionomer film absorbs enough water to dissociate most of the protons, their mobility is governed also by the quality of the phase-separated network; a better connected and less tortuous water-domain network should boost conductivity of a set fraction of dissociated protons (hydronium ions). The degree of phase-separation at max hydration (~95% RH)

follows the same trend as the number of protogenic groups per unit: MASC > PFSA > HPEG. MASC forms a more hydrated (high λ) and better-connected domain-network compared to HPEG, which may translate into higher proton mobility. The fact that we do not observe this effect in the mobility-water fraction trends indicates the ionomer thin films do not possess enough bulk-like water because of confinement (low hydration regime, even at high RH) to realize proton hopping mechanism fully.

- In other words, confinement suppresses the possibly more advantageous nature of MASC ionomers in terms of conductivity to a point where all chemically modified ionomers follow fundamentally a similar proton conduction mechanism, namely vehicular transport and surface mechanism modulate by the ionic moieties. Thus the universal trend (Figure 9d).
- This is not to say MASC ionomers have no advantage overall, because they can still reach higher water uptake and conductivity at high humidity. This implies that these chemical modification routes provide a practically useful means to expand the conductivity-hydration window (over a given humidity range), yet the resulting ionomers are still governed by a fundamentally similar effect mobility-hydration relationship due to strong confinement regime. Thus, this synthesis strategy enables us to alter properties of novel perfluorinated films using a two-prong chemical route (sidechain functional groups and sidechain end groups) while conforming to a universal proton transport relationship which can be harnessed as a design template for functional CL ionomers.

With this two-prong approach, while the conductivity benefits from the addition of imide groups, albeit with a minor impact (MASC > HPEG), it suffers from the elimination of the end-group (PFSA > HPEG). The comparison of their relative impact is not trivial to ascertain, especially in the confinement regime. So, the PFBICE-2 is synthesized in this study to capture both chemical characters. The fact that PFBICE-2 has similar effective conductivity-hydration relationship to PFSA demonstrates that both sidechain end group and functional groups have comparable but opposing influence on film conductivity. In other words, any expected loss in proton transport and reductions in water uptake due to sulfonate replacement is compensated for by additional acid groups/lower EW (697 vs 796 EW). This provides a unique synthesis strategy where one can modulate ionomer film conductivity by means of separate chemical routes.

4.3 Research Directions and Practical Implications

Ionomers have been studied for fuel cell CLs using a variety of methods, including MD simulations[10, 53-55], electrochemical methods for MEAs[58-60], and thin film studies.[12, 23, 27, 32-33, 52, 55] These studies developed an understanding of the application-relevant structure-property relationships for PFSA ionomers, namely: confinement effects, hydration, proton conductivity, oxygen permeability, nanomorphology, and sulfonate-Pt interactions. To overcome the challenges presented by confinement and sulfonate-Pt interactions and improve CL ionomer function, sidechain[22-23] and backbone[4, 17] chemistries have been explored. Hitherto, the chemical origins of these interrelated effects have not been successfully deconvoluted due to a focus on single chemical architecture, like PFSA-based Nafion ionomers. Despite studies on PFSAs with IEC and sidechain variations[11, 18-19, 45, 78], these chemical alterations have not been accomplished in a controlled manner, meaning both IEC (or sidechain separation) and sidechain chemistry have been simultaneously modified. Furthermore, owing to sharing the same characteristic sulfonic acid end group, all these PFSAs modification studies to modulate and mitigate sulfonate-Pt interactions have been limited to materials optimization strategies without precise control over primary synthesis routes.[60, 79-80]

This study remedies this gap by offering a design template for ionomers based on a two-prong approach to alter (i) the sidechain character by adding imide groups to provide additional protogenic species to modulate local acidity in addition to the characteristic SO_3H group, (ii) elimination of the hydrophilic SO_3H group by capping the side chains with hydrophobic groups to modulate the end group-Pt interactions while maintaining the protogenic groups on the side chain. This work systematically explores MASC and HPEG ionomers to provide this understanding. Specifically, this work elucidates how the number of acids per sidechain and the sidechain end group impact application-relevant ionomer properties and structure.

Figure 10 illustrates the impact of MASC and HPEG modifications compared to PFSA and includes a summary of the key findings. While increasing IEC improves water uptake for all chemistries, sidechain functional and end groups impact distribution of water within the mesoscale domain-network (e.g., connectivity and tortuosity), thereby leading to an improved humidity-dependent conductivity for MASC ionomers compared to HPEG ionomers. The effective conductivity exhibits a universal dependence on water volume fraction, which could be attributed to proton conduction driven by primarily by surface mechanism modulated by the ionic moieties in the confinement regime with limited bulk-like water to fully promote the hopping mechanism. Thermal stability and chain mobility also

exhibit linear dependence on IEC but with a secondary effect of chemistry: for a given IEC, HPEG ionomer films exhibit lower transition temperature than MASC. This could be associated with higher chain mobility of HPEG films owing to the absence of the ionic end groups, thereby alleviating the interactions induced by the substrate-SO_3 groups present in MASC and PFSAs. While nanophase separation is improved for MASC ionomers, other morphological features depend more on the sidechain structure (i.e., length and relative location of solvation sites).

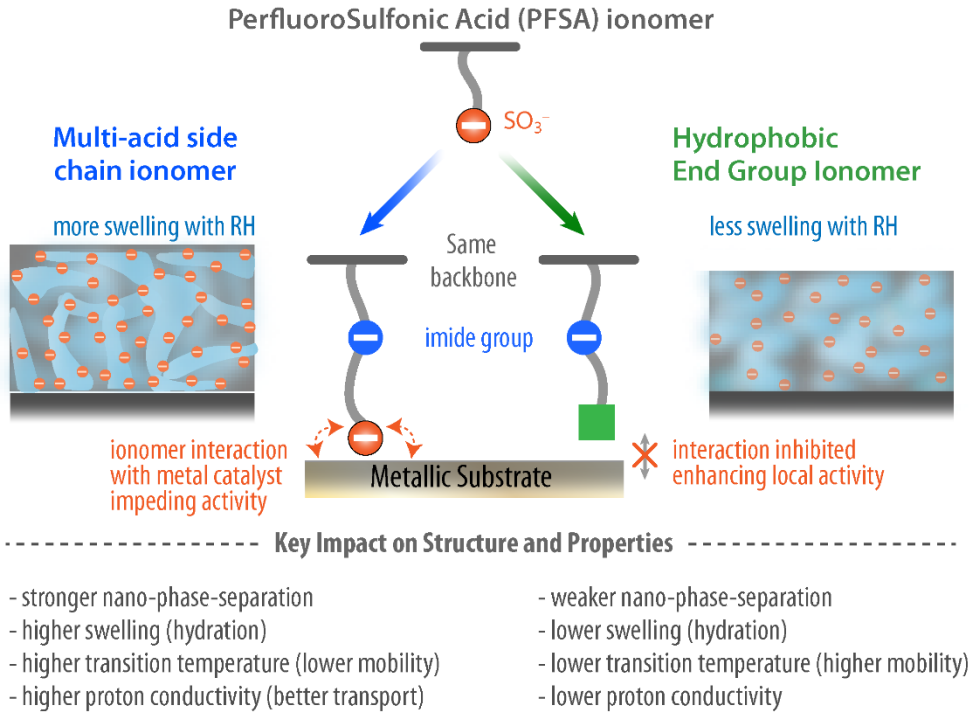

Figure 10. Key findings of sidechain chemistry impact on application-relevant thin film properties, nanomorphology, and functionality.

In brief, the reported chemical strategy for perfluorinated ionomers provides a novel means to modulate substrate interactions, morphology and conductivity, while demonstrating a universal relationship between proton transport and water volume fraction. In addition, chemistry has stronger influence on hydration and nanomorphology of thin films compared to those induced by substrate interactions (Pt or C). Thus, varying ionomer chemistry via end-group and side-chain modifications is a powerful method to independently modulate substrate-ionomer interactions and alter film conductivity

for optimizing CL ionomer function. This work improves the fundamental understanding of chemistry-structure-property relationships of perfluorinated ionomers which have so far been based on PFSAs by providing a novel means to independently control their side-chain and end group and observe the resulting effects on film structure and function.

Conclusion

New and emerging sidechain chemistries provide a way to improve ionomer thin film functionality and overall energy conversion device performance. Additional solvation sites per sidechain increases water uptake, nanophase separation, and ionic interactions, shifting T_α to higher temperature and suggesting greater film stability during thermal treatments in CL fabrication. Interestingly, crystallinity and/or the ionic network limited excessive dimensional swelling for high-IEC ionomers. Therefore, PFICE-2 is perhaps a more viable ionomer due to fewer synthetic steps. Similarly, PFBICE-2 exhibits similar properties to PFSA due competing influence of the two chemical modifications in this study, indicating is PFSA more favorable. Electrochemical methods demonstrate the importance of hydration for proton conduction, but it is important to note that this study used isotropic films, which neglect the impact of domain orientation. Additionally, connectivity and tortuosity impact transport and remain a challenge to characterize. Understanding how to control the ionomer-catalyst interaction is also necessary due to catalyst poisoning. When the ionomers were cast on Pt and C, water uptake and nanomorphology were most sensitive to chemistry rather than substrate. Furthermore, the hydrophobic end groups of PFMI and PFBI also impact the hydrophilic network, leading to the reduced water uptake, which may outweigh the benefits of weakened ionomer-substrate (i.e., catalyst) interactions. Additional studies are necessary to understand the impact of chemistry on the ionomer-substrate interface. Nonetheless, sidechain chemistries allow tuning of ionomer properties and morphology. These results provide insight into phenomena relevant to film function and will guide ionomer design.

Acknowledgement

Authors would like to acknowledge Dr. Peter J. Dudenas and Dr. Adlai Katzenberg for fruitful discussions and insights during data analysis and interpretation. A.B. acknowledges support from the National Science Foundation Graduate Research Fellowship Program under Grant No. DGE 1752814. This work was funded through the Million Mile Fuel Cell Consortium, by the Assistant Secretary for

Energy Efficiency and Renewable Energy, Hydrogen and Fuel Cell Technologies Office, of the U. S. Department of Energy under contract number DE-AC02-05CH11231. This work made use of facilities at the Advanced Light Source (ALS) beamline 7.3.3, supported by the Office of Science, Office of Basic Energy Sciences, of the U.S. Department of Energy (Contract No. DE-AC02-05CH11231)

References

1. Cullen, D. A.; Neyerlin, K. C.; Ahluwalia, R. K.; Mukundan, R.; More, K. L.; Borup, R. L.; Weber, A. Z.; Myers, D. J.; Kusoglu, A., New roads and challenges for fuel cells in heavy-duty transportation. *Nature Energy* **2021,** *6* (5), 462-474.
2. Yandrasits, M. A.; Lindell, M. J.; Hamrock, S. J., New directions in perfluoroalkyl sulfonic acid–based proton-exchange membranes. *Current Opinion in Electrochemistry* **2019,** *18*, 90-98.
3. Kusoglu, A.; Weber, A. Z., New Insights into Perfluorinated Sulfonic-Acid Ionomers. *Chemical Reviews* **2017,** *117*, 987-1104.
4. Jinnouchi, R.; Kudo, K.; Kodama, K.; Kitano, N.; Suzuki, T.; Minami, S.; Shinozaki, K.; Hasegawa, N.; Shinohara, A., The role of oxygen-permeable ionomer for polymer electrolyte fuel cells. *Nat Commun* **2021,** *12* (1), 4956.
5. Cetinbas, F. C.; Wang, X.; Ahluwalia, R. K.; Kariuki, N. N.; Winarski, R. P.; Yang, Z.; Sharman, J.; Myers, D. J., Microstructural Analysis and Transport Resistances of Low-Platinum-Loaded PEFC Electrodes. *Journal of The Electrochemical Society* **2017,** *164*, F1596-F1607.
6. Chen, D.; Kongkanand, A.; Jorne, J., Proton Conduction and Oxygen Diffusion in Ultra-Thin Nafion Films in PEM Fuel Cell: How Thin? *Journal of The Electrochemical Society* **2019,** *166*, F24-F33.
7. Ono, Y.; Ohma, A.; Shinohara, K.; Fushinobu, K., Influence of Equivalent Weight of Ionomer on Local Oxygen Transport Resistance in Cathode Catalyst Layers. *Journal of The Electrochemical Society* **2013,** *160*, F779-F787.
8. Suzuki, T.; Kudo, K.; Morimoto, Y., Model for investigation of oxygen transport limitation in a polymer electrolyte fuel cell. *Journal of Power Sources* **2013,** *222*, 379-389.
9. Weber, A. Z.; Kusoglu, A., Unexplained transport resistances for low-loaded fuel-cell catalyst layers. *J Mater Chem A* **2014,** *2*, 17207-17211.
10. Zhang, X. Y.; Ding, Y. H., Thickness-dependent structural and transport behaviors in the platinum-Nafion interface: A molecular dynamics investigation. *RSC Advances* **2014,** *4*, 44214-44222.
11. Chowdhury, A.; Bird, A.; Liu, J.; Zenyuk, I. V.; Kusoglu, A.; Radke, C. J.; Weber, A. Z., Linking Perfluorosulfonic Acid Ionomer Chemistry and High-Current Density Performance in Fuel-Cell Electrodes. *ACS Appl Mater Interfaces* **2021,** *13* (36), 42579-42589.
12. Eastman, S. A.; Kim, S.; Page, K. A.; Rowe, B. W.; Kang, S.; Soles, C. L.; Yager, K. G., Effect of confinement on structure, water solubility, and water transport in Nafion thin films. *Macromolecules* **2012,** *45*, 7920-7930.
13. Kusoglu, A.; Kushner, D.; Paul, D. K.; Karan, K.; Hickner, M. A.; Weber, A. Z., Impact of substrate and processing on confinement of nafion thin films. *Adv Funct Mater* **2014,** *24*, 4763-4774.
14. Page, K. A.; Kusoglu, A.; Stafford, C. M.; Kim, S.; Kline, R. J.; Weber, A. Z., Confinement-driven increase in ionomer thin-film modulus. *Nano letters* **2014,** *14*, 2299-2304.

15. Tesfaye, M.; Kushner, D. I.; McCloskey, B. D.; Weber, A. Z.; Kusoglu, A., Thermal Transitions in Perfluorosulfonated Ionomer Thin-Films. *ACS Macro Letters* **2018,** *7*, 1237-1242.
16. Jinnouchi, R.; Kudo, K.; Kitano, N.; Morimoto, Y., Molecular Dynamics Simulations on O 2 Permeation through Nafion Ionomer on Platinum Surface. *Electrochimica Acta* **2016,** *188*, 767-776.
17. Katzenberg, A.; Chowdhury, A.; Fang, M.; Weber, A. Z.; Okamoto, Y.; Kusoglu, A.; Modestino, M. A., Highly Permeable Perfluorinated Sulfonic Acid Ionomers for Improved Electrochemical Devices: Insights into Structure-Property Relationships. *Journal of the American Chemical Society* **2020,** *142*, 3742-3752.
18. Garsany, Y.; Atkinson, R. W.; Sassin, M. B.; Hjelm, R. M. E.; Gould, B. D.; Swider-Lyons, K. E., Improving PEMFC Performance Using Short-Side-Chain Low-Equivalent-Weight PFSA Ionomer in the Cathode Catalyst Layer. *Journal of The Electrochemical Society* **2018,** *165*, F381-F391.
19. Kim, O. H.; Oh, S. H.; Ahn, C. Y.; Kim, S.; Kim, J. K.; Kim, J.; Yang, S.; Choi, M.; Cho, Y. H.; Sung, Y. E., Enhanced Performance of Ionomer Binder with Shorter Side-Chains, Higher Dispersibility, and Lower Equivalent Weight. *Fuel Cells* **2018,** *18*, 711-722.
20. Kushner, D. I.; Zhu, L.; Kusoglu, A.; Hickner, M. A., Side Chain Influence on the Mechanical Properties and Water Uptake of Confined Comb-Shaped Cationic Polymer Thin Films. *Macromol Chem Phys* **2016,** *217*, 2442-2451.
21. Su, G. M.; Cordova, I. A.; Yandrasits, M. A.; Lindell, M.; Feng, J.; Wang, C.; Kusoglu, A., Chemical and Morphological Origins of Improved Ion Conductivity in Perfluoro Ionene Chain Extended Ionomers. *Journal of the American Chemical Society* **2019,** *141*, 13547-13561.
22. Yandrasits, M.; Lindell, M.; Schaberg, M.; Kurkowski, M., Increasing fuel cell efficiency by using ultra-low equivalent weight ionomers. *Electrochemical Society Interface* **2017,** *26*, 49-53.
23. Kodama, K.; Motobayashi, K.; Shinohara, A.; Hasegawa, N.; Kudo, K.; Jinnouchi, R.; Osawa, M.; Morimoto, Y., Effect of the Side-Chain Structure of Perfluoro-Sulfonic Acid Ionomers on the Oxygen Reduction Reaction on the Surface of Pt. *ACS Catalysis* **2018,** *8*, 694-700.
24. Kodama, K.; Shinohara, A.; Hasegawa, N.; Shinozaki, K.; Jinnouchi, R.; Suzuki, T.; Hatanaka, T.; Morimoto, Y., Catalyst Poisoning Property of Sulfonimide Acid Ionomer on Pt (111) Surface. *Journal of The Electrochemical Society* **2014,** *161*, F649-F652.
25. Orsino, C. M.; Lindell, M.; Yandrasits, M.; Hamrock, S.; Moore, R. B., Anomalous Appearance of a Distinct Glass Transition in Perfluoroimide Acid Ionomers. *ECS Transactions* **2019,** *92*, 455-466.
26. Schaberg, M. S.; Abulu, J. E.; Haugen, G. M.; Emery, M. A.; O'Conner, S. J.; Xiong, P. N.; Hamrock, S., New Multi Acid Side-Chain Ionomers for Proton Exchange Membrane Fuel Cells. *ECS Transactions* **2019,** *33*, 627-633.
27. Berlinger, S. A.; Dudenas, P. J.; Bird, A.; Chen, X.; Freychet, G.; Mccloskey, B. D.; Kusoglu, A.; Weber, A. Z., Impact of Dispersion Solvent on Ionomer Thin Films and Membranes. *ACS Applied Polymer Materials* **2020**.
28. Gebel, G.; Lambard, J., Small-angle scattering study of water-swollen perfluorinated ionomer membranes. *Macromolecules* **1997,** *30*, 7914-7920.
29. Page, K. A.; Cable, K. M.; Moore, R. B., Molecular origins of the thermal transitions and dynamic mechanical relaxations in perfluorosulfonate ionomers. *Macromolecules* **2005,** *38*, 6472-6484.
30. Kushner, D. I.; Kusoglu, A.; Podraza, N. J.; Hickner, M. A., Substrate-Dependent Molecular and Nanostructural Orientation of Nafion Thin Films. *Adv Funct Mater* **2019,** *29* (37).

31. Roe, R.-J., *Methods of X-Rays and Neutron Scattering in Polymer Science*. Oxford University Press: New York, 2000.
32. Modestino, M. A.; Paul, D. K.; Dishari, S.; Petrina, S. A.; Allen, F. I.; Hickner, M. A.; Karan, K.; Segalman, R. A.; Weber, A. Z., Self-assembly and transport limitations in confined nafion films. *Macromolecules* **2013,** *46*, 867-873.
33. Paul, D. K.; McCreery, R.; Karan, K., Proton Transport Property in Supported Nafion Nanothin Films by Electrochemical Impedance Spectroscopy. *Journal of The Electrochemical Society* **2014,** *161* (14), F1395-F1402.
34. Guo, Y.; Ono, Y.; Nagao, Y., Modification for Uniform Surface of Nafion Ultrathin Film Deposited by Inkjet Printing. *Langmuir* **2015,** *31*, 10137-10144.
35. Sharon, D.; Bennington, P.; Liu, C.; Kambe, Y.; Dong, B. X.; Burnett, V. F.; Dolejsi, M.; Grocke, G.; Patel, S. N.; Nealey, P. F., Interrogation of Electrochemical Properties of Polymer Electrolyte Thin Films with Interdigitated Electrodes. *Journal of The Electrochemical Society* **2018,** *165*, H1028-H1039.
36. Peckham, T. J.; Schmeisser, J.; Rodgers, M.; Holdcroft, S., Main-chain, statistically sulfonated proton exchange membranes: The relationships of acid concentration and proton mobility to water content and their effect upon proton conductivity. *Journal of Materials Chemistry* **2007,** *17*, 3255-3268.
37. Omata, T.; Tanaka, M.; Miyatake, K.; Uchida, M.; Uchida, H.; Watanabe, M., Preparation and fuel cell performance of catalyst layers using sulfonated polyimide ionomers. *ACS Applied Materials and Interfaces* **2012,** *4*, 730-737.
38. Neyerlin, K. C.; Gasteiger, H. A.; Mittelsteadt, C. K.; Jorne, J.; Gu, W., Effect of Relative Humidity on Oxygen Reduction Kinetics in a PEMFC. *Journal ofThe Electrochemical Society* **2005,** *152* (6), A1073-A1080.
39. Xin, L.; Yang, F.; Xie, J.; Yang, Z.; Kariuki, N. N.; Myers, D. J.; Peng, J.-K.; Wang, X.; Ahluwalia, R. K.; Yu, K.; Ferreira, P. J.; Bonastre, A. M.; Fongalland, D.; Sharman, J., Enhanced MEA Performance for PEMFCs under Low Relative Humidity and Low Oxygen Content Conditions via Catalyst Functionalization. *Journal of The Electrochemical Society* **2017,** *164* (6), F674-F684.
40. Shimizu, R.; Park, Y.-C.; Kakinuma, K.; Iiyama, A.; Uchida, M., Effects of Both Oxygen Permeability and Ion Exchange Capacity for Cathode Ionomers on the Performance and Durability of Polymer Electrolyte Fuel Cells. *Journal of The Electrochemical Society* **2018,** *165*, F3063-F3071.
41. Petrovick, J. G.; Radke, C. J.; Weber, A. Z., Gas Mass-Transport Coefficients in Ionomer Membranes Using a Microelectrode. *ACS Meas Sci Au* **2022,** *2* (3), 208-218.
42. Kariuki, N. N.; Haug, A. T.; Park, J. H.; Lindell, M. J.; Myers, D. J., Parametric Study of the Influence of Support Type, Presence of Platinum on Support, and Ionomer Content on the Microstructure of Polymer Electrolyte Fuel Cell Catalyst Layers. *Journal of The Electrochemical Society* **2022,** *169* (10).
43. Katzenberg, A.; Mukherjee, D.; Dudenas, P. J.; Okamoto, Y.; Kusoglu, A.; Modestino, M. A., Dynamic Emergence of Nanostructure and Transport Properties in Perfluorinated Sulfonic Acid Ionomers. *Macromolecules* **2020,** *53*, 8519-8528.
44. Kushner, D. I.; Hickner, M. A., Water Sorption in Electron-Beam Evaporated SiO2 on QCM Crystals and Its Influence on Polymer Thin Film Hydration Measurements. *Langmuir* **2017,** *33*, 5261-5268.
45. Kusoglu, A.; Dursch, T. J.; Weber, A. Z., Nanostructure/Swelling Relationships of Bulk and Thin-Film PFSA Ionomers. *Adv Funct Mater* **2016,** *26*, 4961-4975.

46. Modestino, M. A.; Kusoglu, A.; Hexemer, A.; Weber, A. Z.; Segalman, R. A., Controlling nafion structure and properties via wetting interactions. *Macromolecules* **2012,** *45*, 4681-4688.
47. Yin, C.; Wang, Z.; Luo, Y.; Li, J.; Zhou, Y.; Zhang, X.; Zhang, H.; Fang, P.; He, C., Thermal annealing on free volumes, crystallinity and proton conductivity of Nafion membranes. *Journal of Physics and Chemistry of Solids* **2018,** *120*, 71-78.
48. Kusoglu, A.; Vezzù, K.; Hegde, G. A.; Nawn, G.; Motz, A. R.; Sarode, H. N.; Haugen, G. M.; Yang, Y.; Seifert, S.; Yandrasits, M. A.; Hamrock, S.; Maupin, C. M.; Weber, A. Z.; Di Noto, V.; Herring, A. M., Transport and Morphology of a Proton Exchange Membrane Based on a Doubly Functionalized Perfluorosulfonic Imide Side Chain Perflourinated Polymer. *Chemistry of Materials* **2019,** *32* (1), 38-59.
49. DeCaluwe, S. C.; Kienzle, P. A.; Bhargava, P.; Baker, A. M.; Dura, J. A., Phase segregation of sulfonate groups in Nafion interface lamellae, quantified via neutron reflectometry fitting techniques for multi-layered structures. *Soft Matter* **2014,** *10*, 5763-5776.
50. Dura, J. A.; Murthi, V. S.; Hartman, M.; Satija, S. K.; Majkrzak, C. F., Multilamellar interface structures in Nafion. *Macromolecules* **2009,** *42*, 4769-4774.
51. Kim, S.; Dura, J. A.; Page, K. A.; Rowe, B. W.; Yager, K. G.; Lee, H.-J.; Soles, C. L., Surface-Induced Nanostructure and Water Transport of Thin Proton-Conducting Polymer Films. *Macromolecules* **2013,** *46* (14), 5630-5637.
52. DeCaluwe, S. C.; Baker, A. M.; Bhargava, P.; Fischer, J. E.; Dura, J. A., Structure-property relationships at Nafion thin-film interfaces: Thickness effects on hydration and anisotropic ion transport. *Nano Energy* **2018,** *46*, 91-100.
53. Jinnouchi, R.; Kudo, K.; Kitano, N.; Morimoto, Y., Molecular Dynamics Simulations on O2 Permeation through Nafion Ionomer on Platinum Surface. *Electrochimica Acta* **2016,** *188*, 767-776.
54. Mashio, T.; Malek, K.; Eikerling, M.; Ohma, A.; Kanesaka, H.; Shinohara, K., Molecular dynamics study of ionomer and water adsorption at carbon support materials. *Journal of Physical Chemistry C* **2010,** *114*, 13739-13745.
55. Borges, D. D.; Gebel, G.; Franco, A. A.; Malek, K.; Mossa, S., Morphology of supported polymer electrolyte ultrathin films: A numerical study. *Journal of Physical Chemistry C* **2015,** *119*, 1201-1216.
56. Masuda, T.; Sonsudin, F.; Singh, P. R.; Naohara, H.; Uosaki, K., Potential-dependent adsorption and desorption of perfluorosulfonated ionomer on a platinum electrode surface probed by electrochemical quartz crystal microbalance and atomic force microscopy. *Journal of Physical Chemistry C* **2013,** *117*, 15704-15709.
57. Berlinger, S. A.; McCloskey, B. D.; Weber, A. Z., Probing Ionomer Interactions with Electrocatalyst Particles in Solution. *ACS Energy Letters* **2021,** *6*, 2275-2282.
58. Garrick, T. R.; Moylan, T. E.; Yarlagadda, V.; Kongkanand, A., Characterizing Electrolyte and Platinum Interface in PEM Fuel Cells Using CO Displacement. *Journal of The Electrochemical Society* **2017,** *164*, F60-F64.
59. Kudo, K.; Morimoto, Y., Analysis of Oxygen Transport Resistance of Nafion Thin Film on Pt Electrode. *ECS Transactions* **2013,** *50*, 1487-1494.
60. Van Cleve, T.; Khandavalli, S.; Chowdhury, A.; Medina, S.; Pylypenko, S.; Wang, M.; More, K. L.; Kariuki, N.; Myers, D. J.; Weber, A. Z.; Mauger, S. A.; Ulsh, M.; Neyerlin, K. C., Dictating Pt-Based Electrocatalyst Performance in Polymer Electrolyte Fuel Cells, from Formulation to Application. *ACS Applied Materials and Interfaces* **2019,** *11*, 46953-46964.

61. Ohira, A.; Kuroda, S.; Mohamed, H. F. M.; Tavernier, B., Effect of interface on surface morphology and proton conduction of polymer electrolyte thin films. *Physical Chemistry Chemical Physics* **2013,** *15*, 11494-11500.
62. Tesfaye, M.; MacDonald, A. N.; Dudenas, P. J.; Kusoglu, A.; Weber, A. Z., Exploring substrate/ionomer interaction under oxidizing and reducing environments. *Electrochem Commun* **2018,** *87*, 86-90.
63. Wood, D. L.; Chlistunoff, J.; Majewski, J.; Borup, R. L., Nafion structural phenomena at platinum and carbon interfaces. *Journal of the American Chemical Society* **2009,** *131*, 18096-18104.
64. Mohamed, H. F. M.; Ito, K.; Kobayashi, Y.; Takimoto, N.; Takeoka, Y.; Ohira, A., Free volume and permeabilities of O2 and H2 in Nafion membranes for polymer electrolyte fuel cells. *Polymer* **2008,** *49* (13-14), 3091-3097.
65. Nagao, Y., Proton-Conductivity Enhancement in Polymer Thin Films. *Langmuir* **2017,** *33*, 12547-12558.
66. Liu, Y.; Horan, J. L.; Schlichting, G. J.; Caire, B. R.; Liberatore, M. W.; Hamrock, S. J.; Haugen, G. M.; Yandrasits, M. A.; Seifert, S.; Herring, A. M., A small-angle X-ray scattering study of the development of morphology in films formed from the 3M perfluorinated sulfonic acid ionomer. *Macromolecules* **2012,** *45*, 7495-7503.
67. Chan, J. M.; Wang, M., Visualizing the Orientation of Single Polymers Induced by Spin-Coating. *Nano letters* **2022,** *22* (14), 5891-5897.
68. Selvan, M. E.; He, Q.; Calvo-Muñoz, E. M.; Keffer, D. J., Molecular dynamic simulations of the effect on the hydration of nafion in the presence of a platinum nanoparticle. *Journal of Physical Chemistry C* **2012,** *116*, 12890-12899.
69. Allen, F. I.; Comolli, L. R.; Kusoglu, A.; Modestino, M. A.; Minor, A. M.; Weber, A. Z., Morphology of hydrated as-cast Nafion revealed through cryo electron tomography. *ACS Macro Letters* **2015,** *4*, 1-5.
70. Noguchi, H.; Taneda, K.; Naohara, H.; Uosaki, K., Humidity dependent structure of water at the interfaces between perfluorosulfonated ionomer thin film and Pt and HOPG studied by sum frequency generation spectroscopy. *Electrochem Commun* **2013,** *27*, 5-8.
71. Dudenas, P. J.; Kusoglu, A., Evolution of Ionomer Morphology from Dispersion to Film: An in Situ X-ray Study. *Macromolecules* **2019,** *52*, 7779-7785.
72. Ramaswamy, N.; Kumaraguru, S.; Koestner, R.; Fuller, T.; Gu, W.; Kariuki, N.; Myers, D.; Dudenas, P. J.; Kusoglu, A., Editors' Choice—Ionomer Side Chain Length and Equivalent Weight Impact on High Current Density Transport Resistances in PEMFC Cathodes. *Journal of The Electrochemical Society* **2021,** *168* (2).
73. Choi, P.; Jalani, N. H.; Datta, R., Thermodynamics and Proton Transport in Nafion II. Proton Diffusion Mechanisms and Conductivity. *Journal of the Electrochemical Society* **2005,** *152* (3), E123-E130.
74. Kreuer, K.-D.; Paddison, S. J.; Spohr, E.; Schuster, M., Transport in Proton Conductors for Fuel-Cell Applications: Simulations, Elementary Reactions, and Phenomenology. *Chem Rev* **2004,** *104*, 4637−4678.
75. Paddison, S. J.; Paul, R., The nature of proton transport in fully hydrated Nafion®. *Physical Chemistry Chemical Physics* **2002,** *4* (7), 1158-1163.
76. Eikerling, M.; Kornyshev, A. A.; Kuznetsov, A. M.; Ulstrup, J.; Walbran, S., Mechanisms of Proton Conductance in Polymer Electrolyte Membranes. *Journal of Physical Chemistry B* **2001,** *105* (17), 3646-3662.

77. Kreuer, K.-D., Ion Conducting Membranes for Fuel Cells and other Electrochemical Devices. *Chemistry of Materials* **2013,** *26* (1), 361-380.
78. Shen, S.; Han, A.; Yan, X.; Chen, J.; Cheng, X.; Zhang, J., Influence of Equivalent Weight of Ionomer on Proton Conduction Behavior in Fuel Cell Catalyst Layers. *Journal of The Electrochemical Society* **2019,** *166*, F724-F728.
79. Su, Z.; Kole, S.; Harden, L. C.; Palakkal, V. M.; Kim, C.; Nair, G.; Arges, C. G.; Renner, J. N., Peptide-Modified Electrode Surfaces for Promoting Anion Exchange Ionomer Microphase Separation and Ionic Conductivity. *ACS Materials Letters* **2019,** *1*, 467-475.
80. Kabir, S.; Myers, D. J.; Kariuki, N.; Park, J.; Wang, G.; Baker, A.; Macauley, N.; Mukundan, R.; More, K. L.; Neyerlin, K. C., Elucidating the Dynamic Nature of Fuel Cell Electrodes as a Function of Conditioning: An ex Situ Material Characterization and in Situ Electrochemical Diagnostic Study. *ACS Appl Mater Interfaces* **2019,** *11* (48), 45016-45030.